Applied Surface Science 255 (2009) 7878–7892

Contents lists available at ScienceDirect

Applied Surface Science

journal homepage: www.elsevier.com/locate/apsusc

Some aspects on 3D numerical modeling of high velocity impact of particles in cold spraying by explicit finite element analysis

Wen-Ya Li [a,*], Wei Gao [b]

[a] Shaanxi Key Laboratory of Friction Welding Technologies, School of Materials Science and Engineering, Northwestern Polytechnical University, 127, West Youyi Road, Xi'an, Shaanxi 710072, PR China
[b] State Key Laboratory of Superhard Materials, Jilin University, Changchun 130012, PR China

ARTICLE INFO

Article history:
Received 16 February 2009
Accepted 16 April 2009
Available online 23 April 2009

Keywords:
Cold spraying
Finite element analysis
Copper
Impact behavior
High-speed deformation

ABSTRACT

Three-dimensional modeling of particle impacting behavior in cold spraying by using ABAQUS/Explicit was conducted for copper and other materials. Various combinations of calculation settings concerning material damage, Arbitrary Lagrangian Eulerian adaptive meshing, distortion control and contact interaction were examined. The effects of meshing size and particle size on the impact behavior were analyzed compared to the previous results. The results show that the simulations with material damage cope well with the element excessive distortion and the resultant output is more reasonable than that obtained without material damage. In addition, the meshing size has less effect on the output with the material damage than without material damage. Although particle size has little effect on the morphologies of the deformed particles, it has some effect on the failure of elements at contact interfaces. The critical velocity for particle deposition could be estimated given the appropriate material properties.

1. Introduction

Cold spraying is a coating technology on the basis of aerodynamics and high-speed impact dynamics. In this process, spray particles (usually 5–50 μm in diameter) are accelerated to a high velocity (typically 300–1200 m/s) by a high-speed gas flow that is generated through a convergent–divergent de Laval type nozzle. A coating is formed through the intensive plastic deformation of particles impacting on a substrate at a temperature well below the melting point of the spray material [1]. It has been widely investigated by the experimental method owing to its advantages over the conventional thermal spray processes to deposit a wide variety of metals, alloys and composites [2]. Although it has great application potentials in aerospace, automobile manufacture, chemical industry, etc., there are still some important aspects to be well revealed including the actual bonding mechanism of spray particles.

As for the bonding mechanism of cold spray particles, the most prevailing hypothesis is that plastic deformation may disrupt thin surface films, such as oxides, and provide intimate conformal contact under high local pressure, thus permitting bonding to occur. Accordingly, this bonding process was considered to be comparable to that in a process such as explosive welding or shock wave powder compaction [3–5]. It was also reported that the formation of jetting at the local intensively deformed zones could be helpful in the cleaning of the crushed oxide films [3–8]. The above-mentioned bonding hypothesis is consistent with the fact that a wide range of ductile materials, such as metals and alloys, have been deposited by cold spray and the spray particles experience extensive deformation to form lens-like shapes. Non-ductile materials, such as ceramics, can be only deposited if they are co-cold-sprayed with a ductile (matrix) material or sprayed on a ductile substrate to form a thin layer. This hypothesis can also explain the observed critical velocity necessary to achieve a successful deposition [7–9]. However, there are still some fundamental problems to be revealed, such as the metal jetting and shear instability at the contact interfaces. On the other hand, the observed critical velocity was demonstrated to be influenced by the particle size [5], temperature [4–6,9] and its oxidation state [6,10–12] besides the mechanical properties of the given particle and substrate materials [1,2]. Therefore, it is of significant importance to study the deformation behavior of cold spray particles upon impact.

There are a few studies focused on the impacting and deformation behaviors of spray particles by experiments or simulations. Because of the very short duration of particle impact (tens of nanoseconds), it is very difficult to observe the whole deformation process of particles by experimental inspection. Only

* Corresponding author. Tel.: +86 29 88495226; fax: +86 29 88491426.
E-mail address: liwy@nwpu.edu.cn (W.-Y. Li).

0169-4332/$ – see front matter © 2009 Elsevier B.V. All rights reserved.
doi:10.1016/j.apsusc.2009.04.135

the deformed particles can be observed by a microscope. Therefore, the numerical method takes an important role in studying the particle deformation process. In some studies [3,7], a coupled thermal–mechanical/hydrodynamic (CTH) code, developed at Sandia National Laboratories (Albuquerque, NM, USA) for modeling complex multi-dimensional, multi-problems that are characterized by large deformation and/or strong shocks, was used. This is based on a two-step Eulerian solution algorithm. Two explicit finite element analysis (FEA) softwares, ABAQUS [4,5,8] and LS-DYNA [6,9,10] were also used to investigate the cold spay particle impacting behavior. These two explicit FEA programs are widely used to solve the engineering problems involving in nonlinear dynamic processes.

The reported numerical results in literature [3–10] have indicated that the flattening ratio of particles increases with the increase in particle impact velocity, which is comparable to the experiment results. Moreover, the temperature at localized contact interfaces rises remarkably due to the possible adiabatic shear process. Through numerical simulations by ABAQUS, Assadi et al. [4,5] found that the instability of adiabatic shear flow occurs as particle velocity becomes higher than a critical velocity. Therefore, they took this velocity as the actual critical velocity for particle deposition in cold spray. However, owing to the excessive distortion of elements at the local contact zones in simulation by the Lagrangian algorithm, this calculated critical velocity is much dependent on the meshing size [6,9]. In the previous study [9], when the Arbitrary Lagrangian Eulerian (ALE) method available in LS-DYNA was used to avoid the problems associated with the severe mesh distortion, no steep change of plastic strain or temperature was observed, which was used to indicate the onset of the shear instability by Assadi et al. [4,5]. Accordingly, it seems that the steep change of plastic strain obtained by the Lagrangian method is attributed to the abnormal deformation of elements and cannot be directly associated with the actual shear instability upon particle impacting. In addition, Schmidt et al. [5] also found the dependence of critical velocity on particle size by simulations using ABAQUS with the Lagrangian algorithm. Although the experiments have shown the effect of particle size on critical velocity [5], their simulation results are believed to be unreasonable. The recent studies have shown the effect of particle oxide films on critical velocity [6,10,12]. According to the fact that the powders of small sizes normally have higher oxygen contents than those of large sizes [13], it is expected that the oxide films on particles surfaces are the main factor influencing critical velocity besides the material mechanical properties. However, these views need further experimental study to be clarified.

The above-mentioned results are based on a 2D model. In this study, 3D numerical simulation of particle impacting behavior in cold spraying by using the ABAQUS program was conducted for typical copper material (OFHC) as well as 1100-H12 aluminum alloy. Various combinations of calculation settings concerning material damage, ALE adaptive meshing, contact interaction, etc., were examined with the main focus on the element excessive distortion and its effect on the resultant output. The effects of meshing size and particle size on the impact behavior were also clarified compared to the previous results obtained by using the LS-DYNA code. Some fundamental aspects on 3D modeling of cold spray particle deformation were discussed.

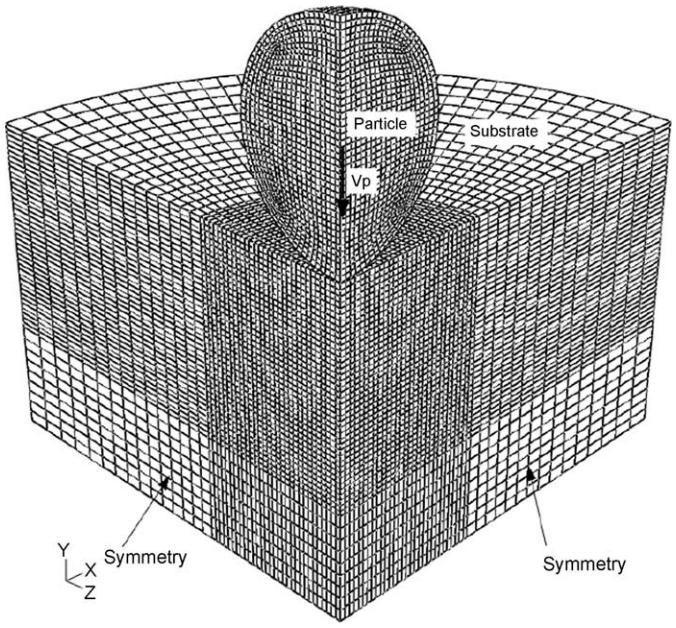

Fig. 1. Computational model with boundary conditions and meshing arrangement (meshing resolution of $1/40d_p$ for a 20 μm particle).

2. Numerical method

The impacting behavior of a particle on a substrate was modeled by using an explicit FEA program ABAQUS/Explicit with the Lagrangian formulation [14]. Owing to the axisymmetric characteristic of normal impact process, a 1/4 symmetric model was used as shown in Fig. 1. In this study, the substrate was taken as a cylinder. For reducing the element number and shortening the calculation time, the radius and height of the substrate were taken to be four and three times larger than the particle radius (e.g., 10 μm). The computational domain was partitioned into several regions for the convenience of meshing and meshed with the gradual change of mesh density (Fig. 1). The meshing was conducted by using the 8-node hexahedral element with coupled displacement and temperature, reduced integration and hourglass control. The nominal meshing size for the particle was 0.5 μm (a meshing resolution of $1/40d_p$) for a 20 μm particle. The interface region in the substrate has the same meshing size as the particle in order to ensure the solution precision. Different meshing sizes and particle sizes were examined as listed in Table 1.

Table 1
Settings of the studied factors in simulations.

Setting factor	Default	Variation
Solution procedure	Dynamic-Temp-Disp-Explicit	No
Hourglass control	Stiffness	No
Distortion control	No	Length ratio: 0.1, 0.4 and 0.8
ALE adaptive meshing	No	Yes, frequency: 10 and 1; remeshing sweeps per increment: 1 and 5
Interface friction	Coefficient of friction (COF): 0.2	COF: 0 and 0.5
Material damage	Yes	No
Meshing size	$1/40d_p$	$1/20d_p$
Particle size	20 μm	80 μm and 20 mm

In the previous studies [4,8], the impacting process was assumed to be an adiabatic process; i.e., the heat transfer is not considered, based on a simple estimation. However, a recent study [5] and our preliminary simulations indicated that heat conduction should be considered in most cases. Therefore, in this study, the available Dynamic-Temperature-Displacement-Explicit procedure (coupled thermal–mechanical analysis) in ABAQUS [14] was used.

The particle/substrate interaction was implemented by using the available surface-to-surface contact (Explicit) formulation in ABAQUS. The contact was controlled to include interior elements surfaces with the nodal erosion to ensure a smooth contact process after the element damage and deletion. In this study, the friction between the particle and substrate was also considered with different coefficients of friction (COFs) (Table 1). The temperature rise is based on the commonly used empirical assumption that 90% of plastic work and 100% friction work is dissipated as heat.

According to our preliminary results, the main setting factors involving in the simulations are summarized in Table 1. It should be pointed out that the element output is element-averaged because the used elements are reduced integration. When one factor is changed, the others take the default settings. In addition, all the simulations are conducted without considering the oxide films and the possible adhesion between the particle and substrate, which will commonly cause the bounce of particle in simulations. This is not the issue to be discussed in this study.

For particles and substrates, the material deformation was described by the Johnson and Cook (JC) plasticity model, which accounts for strain hardening, strain rate hardening and thermal softening effects. The stresses were expressed according to the Von Mises plasticity model. The flow stress (σ) of material is expressed as follows [14,15]:

$$\sigma = (A + B\varepsilon_p^n)\ (1 + C\ln(\dot{\varepsilon}^*))\ (1 - (T^*)^m) \tag{1}$$

where A, B, n, C and m are the constants dependent on materials. ε_p is the effective plastic strain (PEEQ). $\dot{\varepsilon}^*$ is the effective plastic strain rate normalized with respect to a reference strain rate ($\dot{\varepsilon}_p/\dot{\varepsilon}_o$). T^* is a homologous temperature defined as the following [14,15].

$$T^* = \begin{cases} 0 & \text{for} \quad T < T_r \\ (T - T_r)/(T_m - T_r) & \text{for} \quad T_r \le T \le T_m \\ 1 & \text{for} \quad T > T_m \end{cases} \tag{2}$$

where T_m is the melting point and T_r is the reference or transition temperature.

The most important aspect during the simulations of cold spray particle impacting with the Lagrangian algorithm is the possible excessive distortion of elements near the contact surfaces, especially at a higher particle impact velocity. The main measurements to cope with this problem in ABAQUS include ALE adaptive mesh controls, element distortion control and material damage. As reported by Assadi et al. [4], although the ALE adaptive meshing can cope with the excessive element distortion at moderate and high particle impact velocities, frequent remeshing resulted in non-conserving energy variation of the output set, and in unphysical shape of the out-flowing jet of material at the interface. Our preliminary result also shows this fact. In addition, the preliminary results indicate that the large length ratio (nominally from 0 to 1) in element distortion control can also cause the unreasonable shape of the deformed particle similar to that obtained with the ALE adaptive meshing.

It is worth noting that the element deletion based on the damage model can lead to an important influence on the deformed particle shape and the output. These results will be given in the following section. The Johnson and Cook damage model (referred to as the "Johnson-Cook dynamic failure model" in ABAQUS) was used, which accounts for the effects of hydrostatic pressure, strain rate and temperature [14,15]. ABAQUS/Explicit also offers a more general implementation of the JC failure model as part of the family of damage initiation criteria, which is the recommended technique for modeling progressive damage and failure of materials. The JC dynamic failure model is based on the value of the equivalent plastic strain at element integration points, where failure is assumed to occur when the damage parameter exceeds 1. The damage parameter, ω, is defined as

$$\omega = \sum \left(\frac{\Delta \bar{\varepsilon}_p}{\bar{\varepsilon}_{pf}} \right) \tag{3}$$

where $\Delta\bar{\varepsilon}_p$ is an increment of the equivalent plastic strain, $\bar{\varepsilon}_{pf}$ is the strain at failure, and the summation is performed over all increments in the analysis. The strain at failure is assumed to be dependent on a nondimensional plastic strain rate, $\dot{\varepsilon}^*$; a dimensionless pressure-deviatoric stress ratio, p/q (where p is the pressure stress and q is the Mises stress); and the nondimensional temperature, T^*, defined earlier in the JC plasticity model. The dependencies are assumed to be separable and are of the form

$$\bar{\varepsilon}_{pf} = \left[d_1 + d_2 \exp\left(d_3 \frac{p}{q} \right) \right] [1 + d_4 \ln(\dot{\varepsilon}^*)](1 + d_5 T^*) \tag{4}$$

where d_1–d_5 are failure parameters measured at or below the transition temperature, T_r. When this failure criterion is met, the deviatoric stress components are set to zero and remain zero for the rest of the analysis. Depending on the selected values, the pressure stress may also be set to zero for the rest of calculation (if this is the case, it must be specified element deletion and the element will be deleted) or it may be required to remain compressive for the rest of the calculation (if this is the case, it must be chosen not to use element deletion). By default, the elements that meet the failure criterion are deleted. It can be specified the fracture energy per unit area, G_f, to be dissipated during the damage process directly, which means defining damage evolution based on energy dissipated in ABAQUS. Instantaneous failure will occur if G_f is specified as 0. However, this choice is not recommended and should be used with care because it causes a sudden drop in the stress at the material point that can lead to dynamic instabilities. Therefore, the evolution in the damage was specified in exponential form in this study. Other detailed information can be found in the ABAQUS Analysis User's Manual [14].

Because of the excellent cold sprayability of copper, it has been widely studied experimentally. In this study, Cu was employed as the objective material based on its easily available material data (e.g., [15]) used in simulations as shown in Table 2. 1100-H12 aluminum alloy was also studied because of the available material properties [16] (Table 2). The mechanical and thermal material properties were assumed to be isotropic. It was also assumed that the initial temperatures of particle and substrate (T_o) are 25 °C. The initial velocity of particle (v_p) is dependent on the conditions to be study.

3. Results and discussion

3.1. Simulation results without material damage

3.1.1. Without ALE adaptive meshing

Fig. 2 shows the typical simulation results for a 20 μm Cu particle impacting on Cu substrate at 300 m/s obtained without material damage and ALE adaptive meshing, and with a COF of 0.2 and a meshing size of 0.5 μm. The procedure finished normally at 60 ns. As reported in literature [4,8–10], it is seen from Fig. 2a that a crater is developed in the substrate as the particle impinges the substrate. The plastic deformation in the particle and substrate is

Table 2
Properties of OFHC copper [15] and 1100-H12 aluminum alloy [16] used in simulations.

Parameter	Cu	Al1100
Density, kg/m^3	8960	2700
Thermal conductivity, W/(m °C)	386	220
Specific heat, J/kg °C	383	920
Melting point, °C	1083	620
Elastic modulus, GPa	124	65.762
Poisson's ratio	0.34	0.3
JC plasticity: A, MPa, B, MPa, n, C, m	90, 292, 0.31, 0.025, 1.09	148.361, 345.513, 0.183, 0.001, 0.859
JC damage: d_1, d_2, d_3, d_4, d_5	0.54, 4.89, −3.03, 0.014, 1.12	0.071, 1.248, −1.142, 0.147, 1.0[a]
Reference temperature, °C	25	20
Reference strain rate, 1/s	1	1

[a] *Note*: In Ref. [16], m is set as zero without taking into account the effect of temperature on damage. Here, we give a moderate value of 1. In addition, d_1 seems a little small for Al1100.

concentrated in a narrow region surrounding the particle/substrate interface. The plastic strain of certain interfacial element increases rapidly to a high value as the progressing of impacting, suggesting the localized deformation (Fig. 2c). But no interfacial metal jet is observed under this low velocity condition. The strain rate is extremely high and could be 10^8 to 10^9 1/s (Fig. 2d), which is comparable to the previously predicted values by others [4,8]. This strain value is even higher than the so-called super-high strain rate in engineering fields (10^4 to 10^6 1/s). Due to localization of the plastic deformation, a significant temperature rise is observed in the interface region (Fig. 2b). However, the maximum temperature rise is much lower than the previously predicted values [4,8,9] owing to the obvious heat conduction from the interface to the inner particle and substrate, especially for Cu of high conductivity. Therefore, the present result clarifies this point of view that heat conduction should be considered in the simulations of cold spray particles impacts. In addition, the energy evolution (Fig. 2e) clearly shows that during the impacting process, the kinetic energy of particle is converted into internal energy (e.g., frictional dissipation, plastic dissipation and recoverable strain energy), and part of which changes into heat at the deformed zones. These facts are consistent with the previous results obtained with the 2D axisymmetric model.

As the increase of particle impact velocity, the particle deformation extent increases obviously with much increased interfacial plastic strain (Fig. 3a and c) and temperature rise (Fig. 3b). The interfacial metal jet is clearly observed at 500 m/s (Fig. 3c). However, the program could not normally finish due to

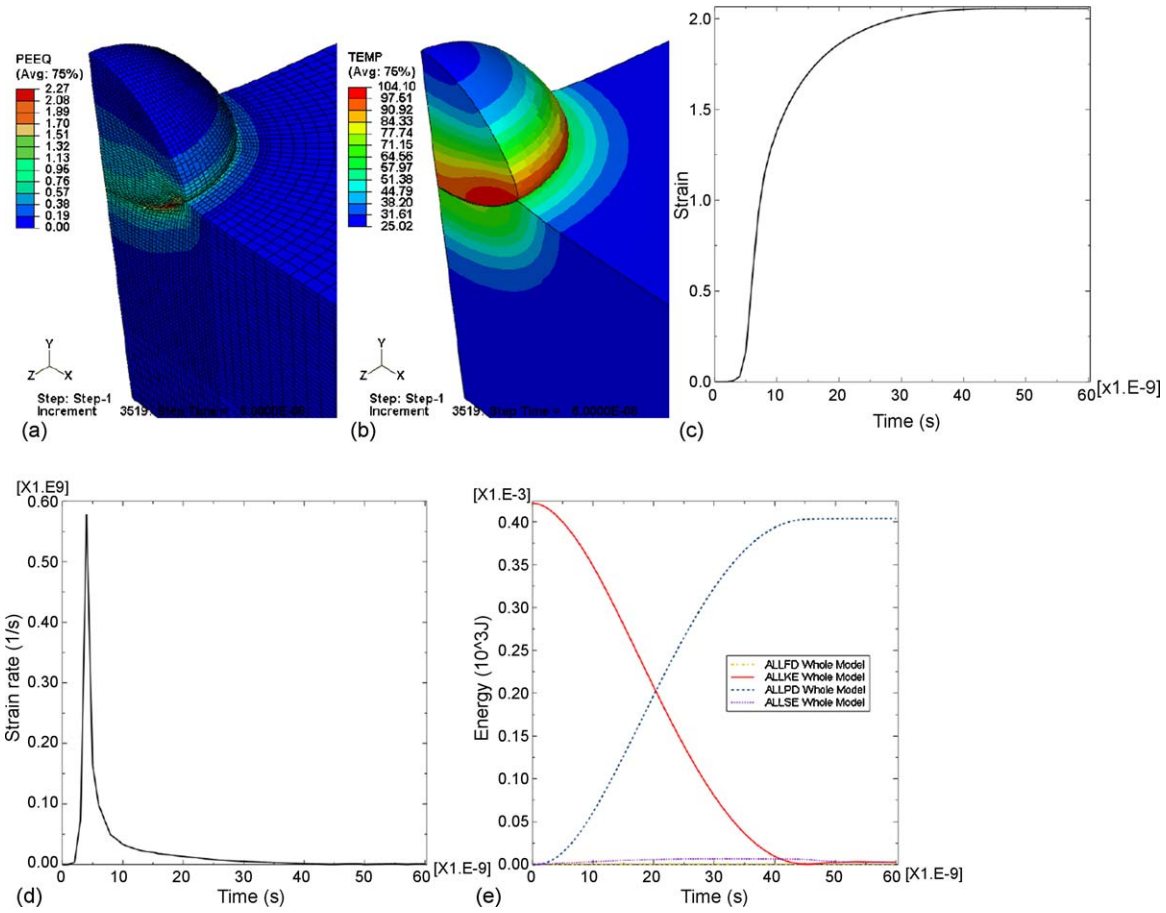

Fig. 2. Simulated contours of PEEQ (a) and temperature (b), and temporal evolutions of PEEQ (c) and strain rate (d) of an interfacial element at the particle surface, and energy (e) for a 20 μm Cu particle. Computed without material damage and ALE adaptive meshing, with a COF of 0.2 and at an impact velocity of 300 m/s. Note that ALLFD is frictional dissipation, ALLKE is kinetic energy, ALLPD is plastic dissipation and ALLSE is recoverable strain energy.

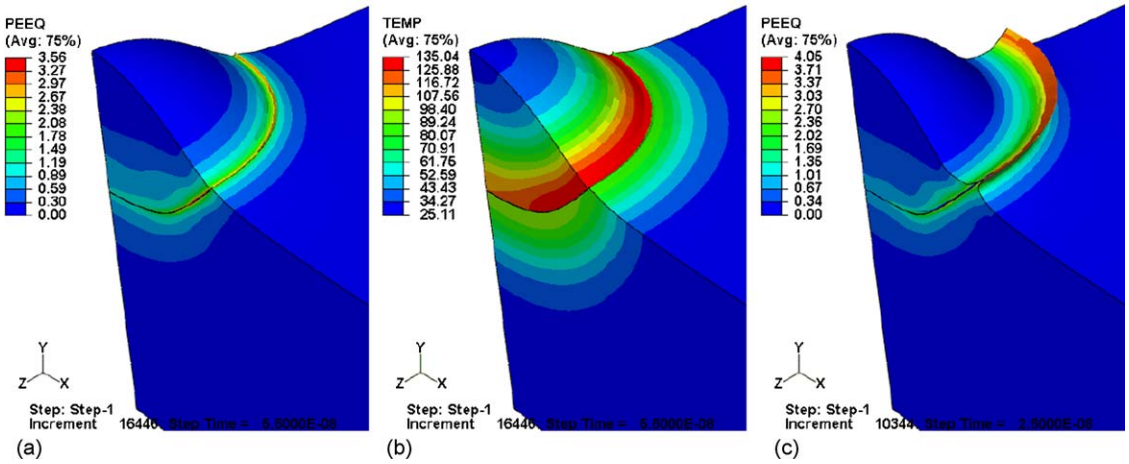

Fig. 3. Simulated contours of PEEQ (a and c) and temperature (b) for a 20 μm Cu particle impacting at 400 m/s (a and b) and 500 m/s (c). Computed without material damage and ALE adaptive meshing, with a COF of 0.2. Note that the program failed at around 57 ns for impacting at 400 m/s (almost finished at 60 ns and the particle has started to rebound); the program failed at around 27 ns for impacting at 500 m/s.

the excessive distortion of elements near the contact surfaces, especially at a higher particle impact velocity. For example, the program failed at around 57 ns at 400 m/s (almost finished at 60 ns and the particle has started to rebound) and terminated at about 27 ns at 500 m/s. This is the potential problem inherent to the Lagrangian algorithm as indicated before [9]. The excessive distortion of elements will yield the unfaithful output, and even worse, terminate the program. Therefore, ALE technique was used to deal with this essential problem [4,9]. In addition, material damage and distortion control techniques available in ABAQUS can also be employed.

3.1.2. With ALE adaptive meshing

The ALE adaptive meshing technique in ABAQUS combines the features of pure Lagrangian analysis and pure Eulerian analysis. It is a tool that makes it possible to maintain a high-quality mesh throughout an analysis, even when large deformation or loss of material occurs, by allowing the mesh to move independently of the material [14]. However, in some extreme cases, it does not work well [14]. Based on the preliminary results, just frequency and remeshing sweeps per increment were considered with other settings as default in this study. The results show that, for a 20 μm Cu particle impacting at 500 m/s, the simulations with the ALE adaptive meshing and a meshing size of $1/40d_p$ but without material damage could not finished normally, no matter what combination of remeshing frequency and sweeps were used. Fig. 4 shows the typical simulation result obtained with the remeshing frequency and sweeps per increment as 1 and 10, respectively. Although the elements shapes were good, the program failed earlier at about 9 ns compared to the result without the ALE adaptive meshing (Fig. 3c). The high strain rate during cold spraying is the extreme case. Therefore, ALE adaptive meshing may be combined with other techniques, such as material damage, to make it work in modeling cold spray particle impacts.

3.1.3. With distortion control

Fig. 5 shows the typical results for a 20 μm Cu particle impacting at 500 m/s obtained without material damage and ALE adaptive meshing but distortion controls having different length ratios (0.1, 0.4 and 0.8). It is noticed that the program using the length ratio of 0.1 failed at about 30 ns (Fig. 5a), and failed at around 33 ns with the length ratio of 0.4 (Fig. 5b). The program successfully finished at 60 ns with the length ratio of 0.8, but the resultant particle shape is a little unrealistic with the smooth margins (Fig. 5c). Therefore, similar to the ALE adaptive meshing, distortion control is not quite suitable for modeling cold spray particle impacts.

3.1.4. Effect of meshing size

As indicated in the previous studies [6,9], the meshing size has significant effect on the simulation results with the pure Lagrangian algorithm. As expected, the program could normally finish for a 20 μm Cu particle impacting at 500 m/s computed with a meshing size of 1 μm ($1/20d_p$) and without material damage and ALE adaptive meshing as shown in Fig. 6. The resultant particle and crater shapes are comparable to those obtained with a 2D model [9], but the evolutions of plastic strain and temperature are different. This result further proves the influence of meshing size on computation accuracy. In the following, the effect of material

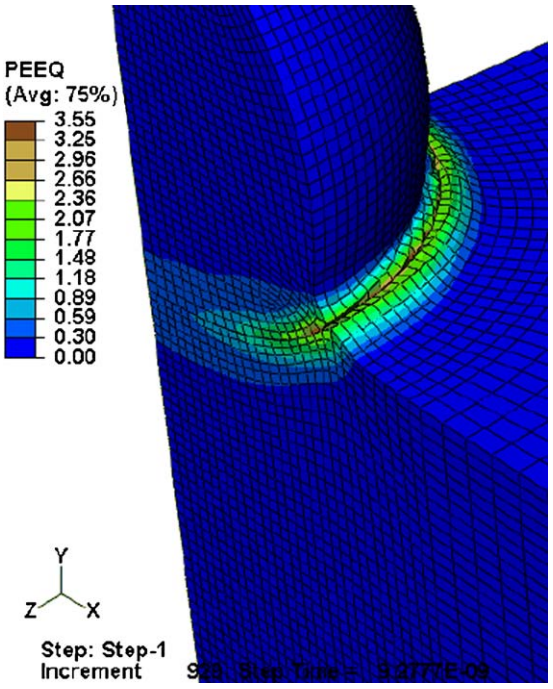

Fig. 4. Simulated contour of PEEQ for a 20 μm Cu particle impacting at 500 m/s. Computed without material damage but with ALE adaptive meshing and a COF of 0.2. The remeshing frequency and sweeps per increment are 1 and 10, respectively. Note that the program failed at around 9 ns.

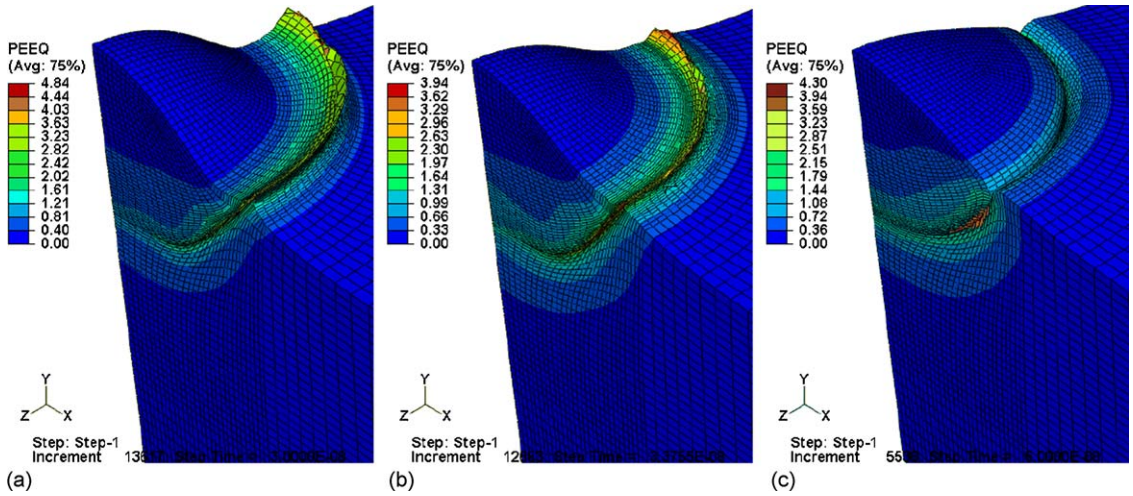

Fig. 5. Simulated contours of PEEQ for a 20 μm Cu particle impacting at 500 m/s. Computed without material damage and ALE adaptive meshing, and with a COF of 0.2 and distortion controls having length ratios of 0.1 (a), 0.4 (b) and 0.8 (c). Note that the program using the length ratio of 0.1 failed at about 30 ns, and failed at around 33 ns with the length ratio of 0.4.

damage in modeling cold spray particle impacts will be discussed in detail.

3.2. Simulation results with material damage

Although the above-mentioned calculation techniques can be performed successfully to yield some comparable output, sometimes they do not work well; e.g., when the meshing size is relatively fine which can possibly result in more precise data. Therefore, the material failure model with the present 3D model was examined for the first time in this study according to the suggestion documented in the ABAQUS manual [14]. In the preliminary study with a 2D axisymmetric model using ABAQUS, it was found that the resultant particle shape with material damage seemed more reasonable. However, some results were not satisfactory owing to the unrealistic deformation of substrate elements at the interface, which cannot be set with material damage as the master surface in a 2D model [14]. As a result, the 3D modeling was conducted, where the erosion contact is permitted in ABAQUS [14].

3.2.1. Typical results with material damage

Fig. 7 shows the representative result for a 20 μm Cu particle impacting at 500 m/s simulated with material damage and a COF of 0.2 but without ALE adaptive meshing. It is seen that under this moderate impact velocity the elements of large deformation in the particle and substrate near the contact interface have been deleted and the particle has penetrated into the substrate (Fig. 7a). Similar to the above-mentioned results, the intensive plastic deformation is concentrated at the narrow interfacial region. The temperature rise and heat conduction is also obviously observed (Fig. 7b). In addition, the deformed shape is to some what different from that obtained without material damage (Fig. 6a). No clear metal jet is formed because of the deletion of failure elements. However, the resultant particle shape with material damage seems reasonable as compared to the experiments [4,9]. Moreover, it is noticed from the energy evolution (Fig. 7c) that the apparent residual kinetic energy is higher and the plastic dissipation is lower compared to the results obtained without material damage. The higher kinetic energy is attributed to the deletion of the damaged elements from the calculation, while they possess part of the whole kinetic

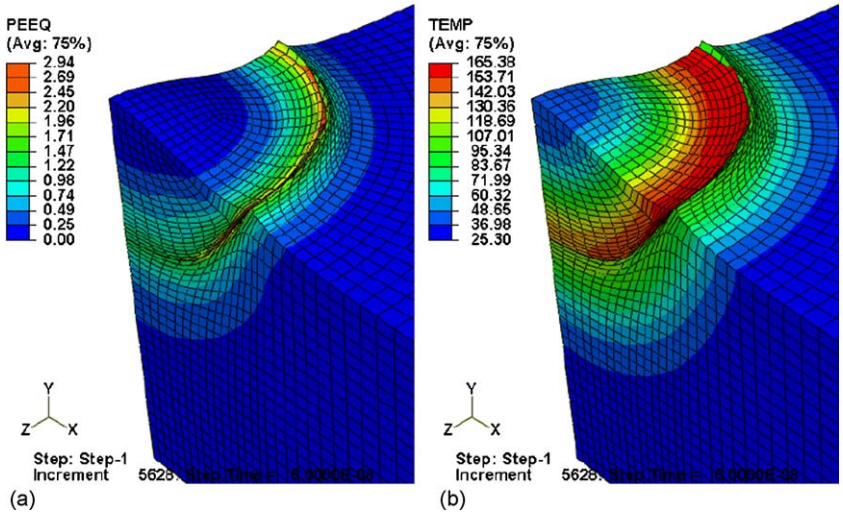

Fig. 6. Simulated contours of PEEQ (a) and temperature (b) for a 20 μm Cu particle impacting at 500 m/s. Computed without material damage and ALE adaptive meshing, with a COF of 0.2 and a meshing size of 1 μm ($1/20d_p$).

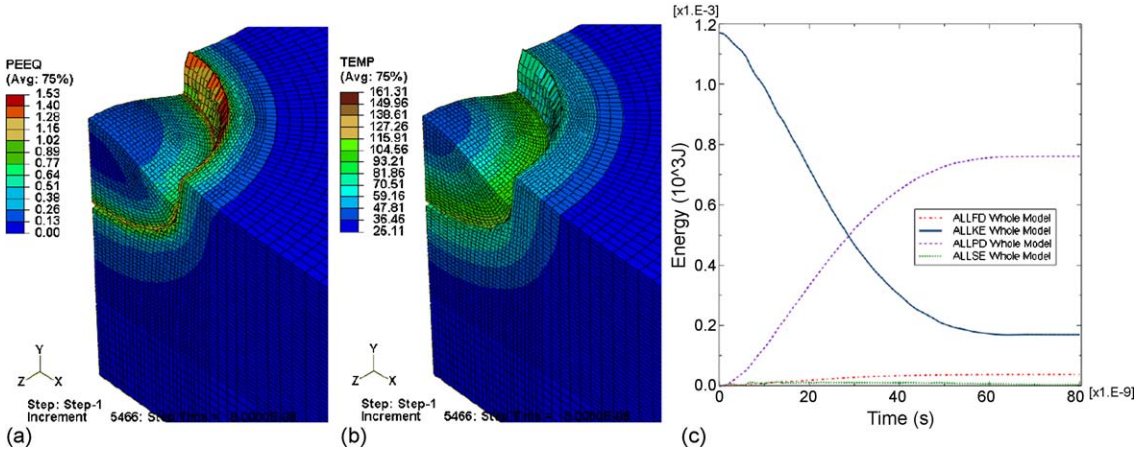

Fig. 7. Simulated contours of PEEQ (a) and temperature (b), and temporal evolution of energy or work dissipation (c) for a 20 μm Cu particle impacting at 500 m/s. Computed without ALE adaptive meshing, with material damage and a COF of 0.2. Note that ALLFD is frictional dissipation, ALLKE is kinetic energy, ALLPD is plastic dissipation, and ALLSE is recoverable strain energy.

energy. The lower plastic dissipation is caused by the limitation of plastic strain with material failure.

Fig. 8 illustrates the front view of the particle contact surface at different contact times for a 20 μm Cu particle impacting at 500 m/s. It is clearly seen that some elements have started to be deleted at about 3 ns (Fig. 8b) because they meet the damage criteria described by Eq. (3). As the contact time increase, more elements are quickly deleted until about 30 ns (Fig. 8g). And then, the impacting process tends to the end as can be reflected by the unchanged maximum plastic strain from 30 to 80 ns (Fig. 8g–i).

3.2.2. Effect of ALE adaptive meshing

For comparison, the simulations with both material damage and ALE adaptive meshing were conducted under different combination of remeshing frequency and sweeps. It is interestingly found that the ALE adaptive meshing has little effect on the results under the studied combinations of remeshing frequency (from 1 to 50) and sweeps (from 1 to 10). Fig. 9 shows a typical simulated result with the remeshing frequency and sweeps per increment as 1 and 1, respectively. Compared to those without ALE adaptive meshing (Fig. 7a and b), the particle shape, plastic strain and temperature are almost identical. Therefore, the ALE adaptive meshing is not necessarily required when using material damage in modeling the cold spray particle impacts.

3.2.3. Effect of interface friction

Another consideration in this study is the interfacial friction based on the preliminary study with the 2D model and without material damage, where the friction takes a little role in simulations. In the previous study on particle/substrate interaction, no friction between the particle and substrate was considered [4–10]. Therefore, friction was included for the first time in this study by using the available friction models in ABAQUS. There are several friction models in ABAQUS, such as the basic Coulomb friction model, shear stress versus elastic slip while sticking, exponential decay friction model [14]. As a first approximation, the simple Coulomb friction model was used in this study.

Fig. 10 shows the simulation results obtained with the COFs of 0 and 0.5. Compared with the result obtained with the COF of 0.2 (Fig. 7), it is found that the resultant particle shapes are almost the same. The maximum PEEQ and temperature rise at the interface have a little variation but irregular. In addition, the energy change also presents similar under different COFs (Fig. 10c, Fig. 7c, Fig. 10f). That means the friction has a little effect on the resultant output when changed from 0 to 0.5. This is attributed to the much higher kinetic energy compared to the friction dissipation as well as the consideration of material damage. Therefore, in the following investigation, a small COF of 0.2 is used in modeling cold spray particles impacts because it may be appropriate in practice with a little friction.

3.2.4. Effect of particle impact velocity

Using the above developed solution procedure, i.e., with material damage and a COF of 0.2 but without ALE adaptive meshing, the effect of particle impact velocity was reconsidered. Fig. 11 shows the simulated contours of PEEQ and temperature for a 20 μm Cu particle impacting at different velocities. In addition to the result obtained at the impact velocity of 500 m/s as shown in Fig. 7a and b, it is seen that with increasing the impact velocity from 200 to 800 m/s the particles have deformed more extensively with the decrease of height of the residual particle (Fig. 11a–f). The depth of crater increases with the increase of impact velocity. The particles have obviously penetrated into the substrate as the impact velocity higher than 400 m/s. On the other hand, the maximum temperature rise also augments with increasing the particle velocity (Fig. 11g–l). These results are consistent with the reported results in literature [3–9]. It is also noticed that the interfacial temperature rise is not as higher as the reported ones, even at a high impact velocity. For example, it is about 146 °C at 800 m/s; while the reported values could reach the melting point of Cu [3,4,8]. The relatively low temperature rise could be attributed to the deletion of the damaged elements which possess a relatively high temperature. Nevertheless, take into account that the real temperature at the interface of Cu particle and substrate may not be high and the damage is believed to occur in the real impact process, the finding on temperature rise in this study should be reasonable. This deserves a further study. The results also agree with the fact that the impact erosion will occur in cold spraying, especially at a high impact velocity, as experimentally observed by Schmidt et al. [5].

Furthermore, another important issue is found that the deletion of elements occurs as the impact velocity is not less than 250 m/s. This fact may be associated with the particle critical velocity and will be discussed in detail allied with the following results in the following section.

3.2.5. Effect of meshing size

As above-mentioned and previously reported [6,9] using the LS-DYNA code that the meshing density takes an important role in the computation with the Lagrangian algorithm and influences

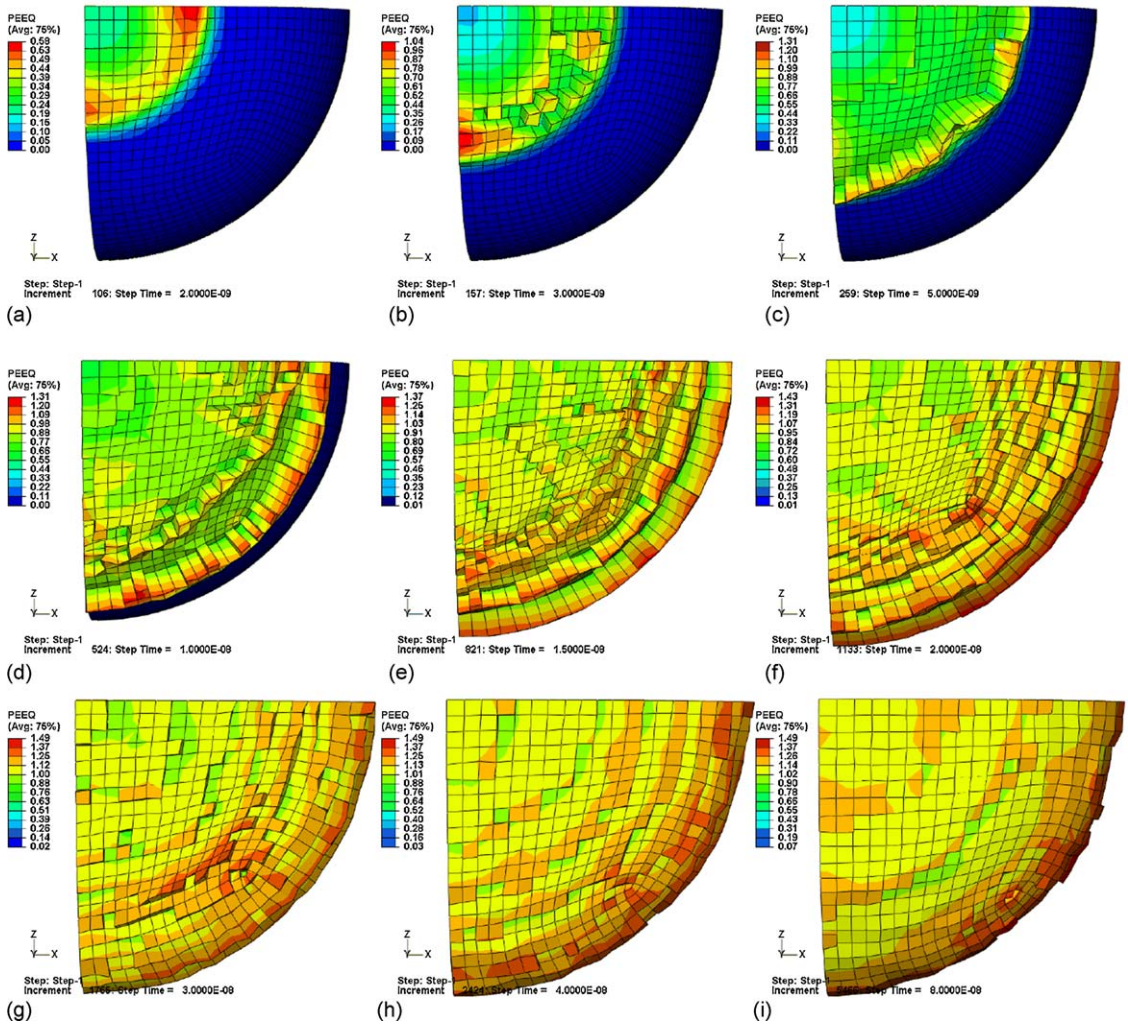

Fig. 8. Typical temporal evolution of PEEQ at the contact surface of particle for a 20 μm Cu particle impacting at 500 m/s. Computed without ALE adaptive meshing, with material damage and a COF of 0.2. (a) 2 ns, (b) 3 ns, (c) 5 ns, (d) 10 ns, (e) 15 ns, (f) 20 ns, (g) 30 ns, (h) 40 ns and (i) 80 ns.

significantly the resultant output. Although Assadi et al. [4] have recognized this using ABAQUS/Explicit, they did not explore this effect and present the effective measures to cope with it. Therefore, the previous study [6,9] showed some validation and explanation on the effect of the relative meshing size. The excessive distortion of elements is contributed to this influence taking into account the fact that the output is element-averaged [6,9]. Therefore, just take the onset velocity of excessive element distortion under certain

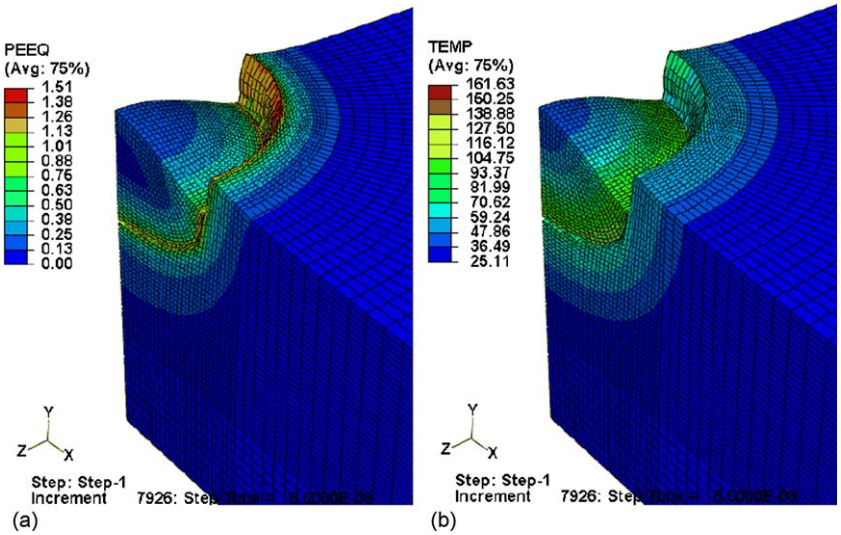

Fig. 9. Simulated contours of PEEQ (a) and temperature (b) for a 20 μm Cu particle impacting at 500 m/s. Computed with material damage, ALE adaptive meshing and a COF of 0.2. The remeshing frequency and sweeps per increment are 1 and 1, respectively.

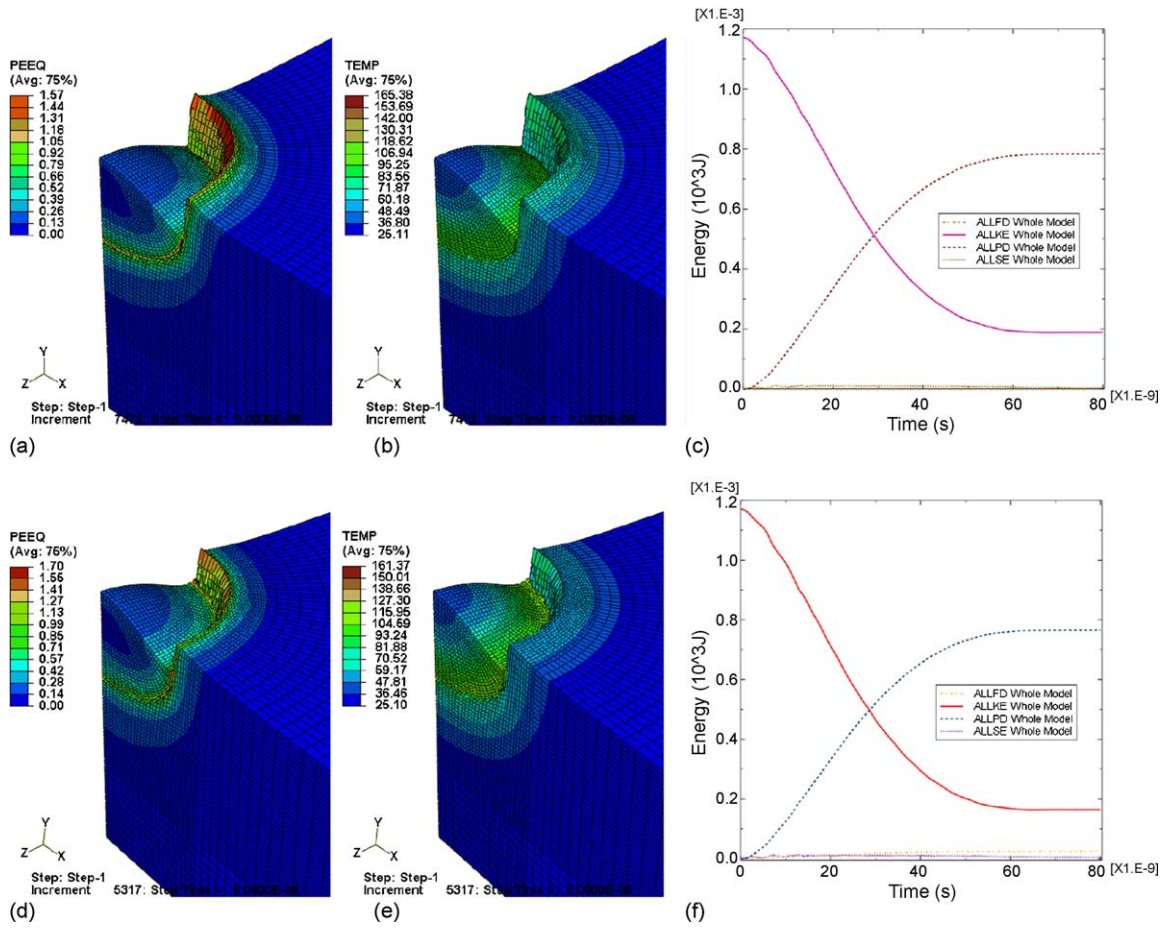

Fig. 10. Simulated contours of PEEQ (a and d) and temperature (b and e), and temporal evolution of energy or work dissipation (c and f) for a 20 μm Cu particle impacting at 500 m/s. Computed without ALE adaptive meshing, with material damage and COFs of 0 (a, b, and c) and 0.5 (d, e, and f). Note that ALLFD is frictional dissipation, ALLKE is kinetic energy, ALLPD is plastic dissipation, and ALLSE is recoverable strain energy.

meshing size is lack of evidence. The extrapolation of the data obtained under different meshing sizes to a zero element size yielded a reasonable critical velocity of about 300 m/s for Cu [9] and has been supported by experiments [5,6]. In this study, since the material damage technique was used, the effect of meshing size was further examined under this condition.

Fig. 12 shows the simulated contours of PEEQ for a 20 μm Cu particle impacting at the velocities from 200 to 600 m/s. The computation was conducted with material damage, a COF of 0.2 and a meshing size of 1 μm, but without ALE adaptive meshing. Compared to the results obtained with the meshing size of 0.5 μm as shown in Fig. 7a, Fig. 11a–e, the morphologies of the deformed particles are almost the same with a little variation of maximum plastic strain under a given impact velocity. As the increase of particle impact velocity, the deformation extent is enhanced obviously, especially at high velocities (Fig. 12d and e). This fact clearly shows that the meshing size influence much less the resultant output with the material damage technique than without it. This result also means that one may obtain more reasonable data with material damage. In addition, it is interesting to find that the deletion of elements also occurs as the impact velocity is 250 m/s. This fact may further prove the less effect of meshing size compared to those obtained without material damage. The prediction of particle critical velocity by the modeling method used in this study will be discussed in the following section.

3.2.6. Effect of particle size

In the previous study on the effect of particle size on its deformation behavior with the 2D model using LS-DYNA [9], it was found that the deformation of different particles having various sizes present a similarity if the meshing sizes are relatively the same, i.e., with the same meshing resolution (e.g., $1/32d_p$ [9]). However, Schmidt et al. [5] found the effect of particle size on critical velocity for copper and 316L powders by the experimental method. They did not clarify the underlying mechanism. The recent studies have shown the effect of particle surface oxide films on critical velocities of Cu [6] and Al [10,12]. According to the fact that the powders of small sizes normally have higher oxygen contents than those of large sizes [13], it is considered that the oxide films on particles surfaces, not the particle size, is the main factor influencing critical velocity besides the material mechanical properties. The previous study showed that the critical velocities of Cu having different sizes but belonging to the same stock (almost oxygen free in a vacuum tank) present the similarly low critical velocities [6]. However, these views need further experimental study to be clarified. In this study, the effect of particle size was analyzed with the developed 3D model.

Figs. 13 and 14 show the simulation results for 80 μm and extremely 20 mm Cu particles impacting at different velocities computed with material damage and a meshing resolution of $1/40d_p$. Compared to the results of a 20 μm Cu particle (Fig. 7a, Fig. 11a–e), the shapes of the deformed particles are almost the same with a little variation of maximum plastic strain under a given impact velocity. Similarly, as the increase of particle impact velocity, the deformation extent is remarkably increased. These results apparently indicate that the particle size influence little the resultant output with the material damage technique as found before [9]. However, through a careful examination of the

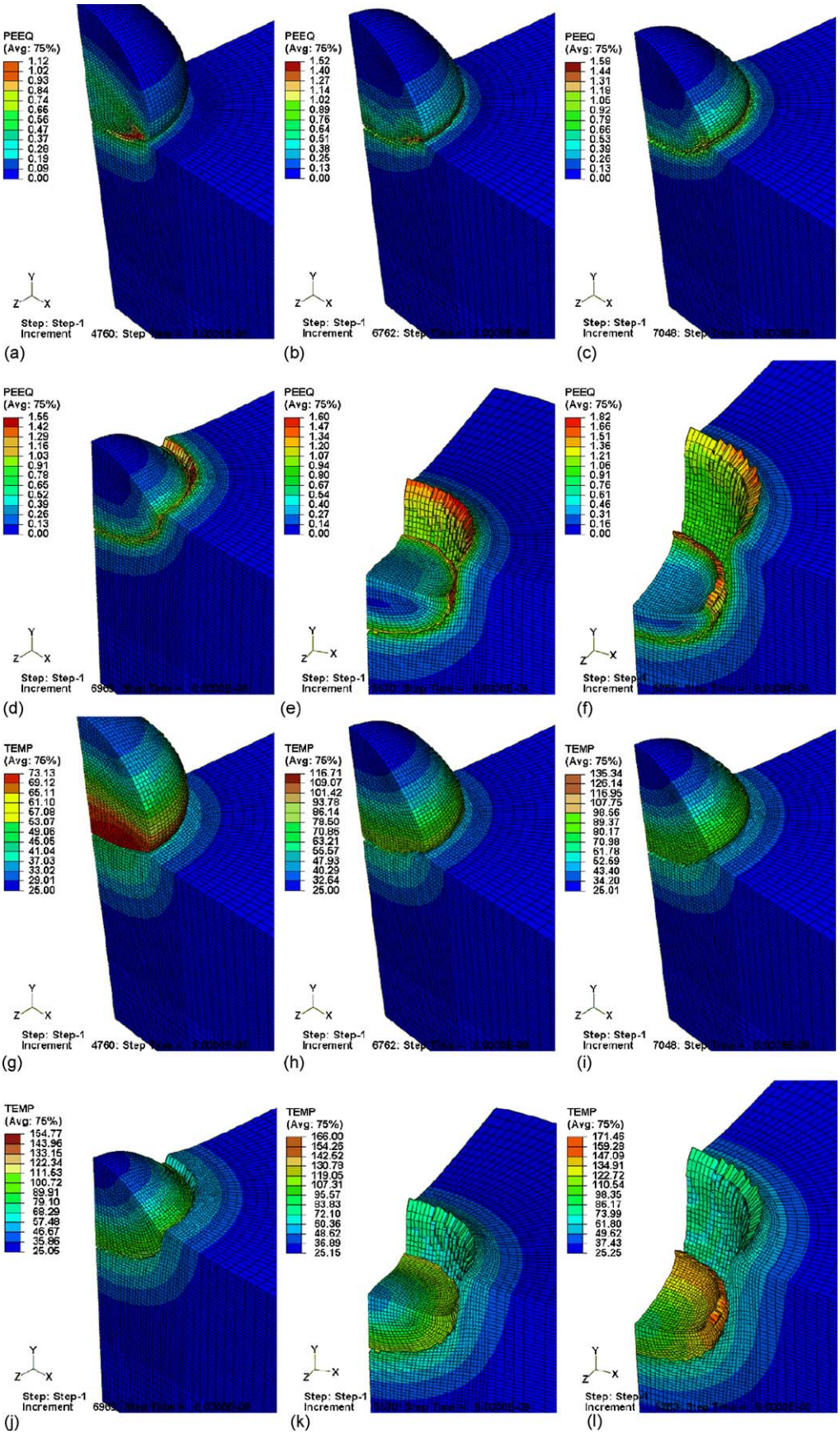

Fig. 11. Simulated contours of PEEQ (a–f) and temperature (g–l) for a 20 μm Cu particle impacting at 200 m/s (a and g), 250 m/s (b and h), 300 m/s (c and i), 400 m/s (d and j), 600 m/s (e and k) and 800 m/s (f and l). Computed without ALE adaptive meshing, with material damage and a COF of 0.2.

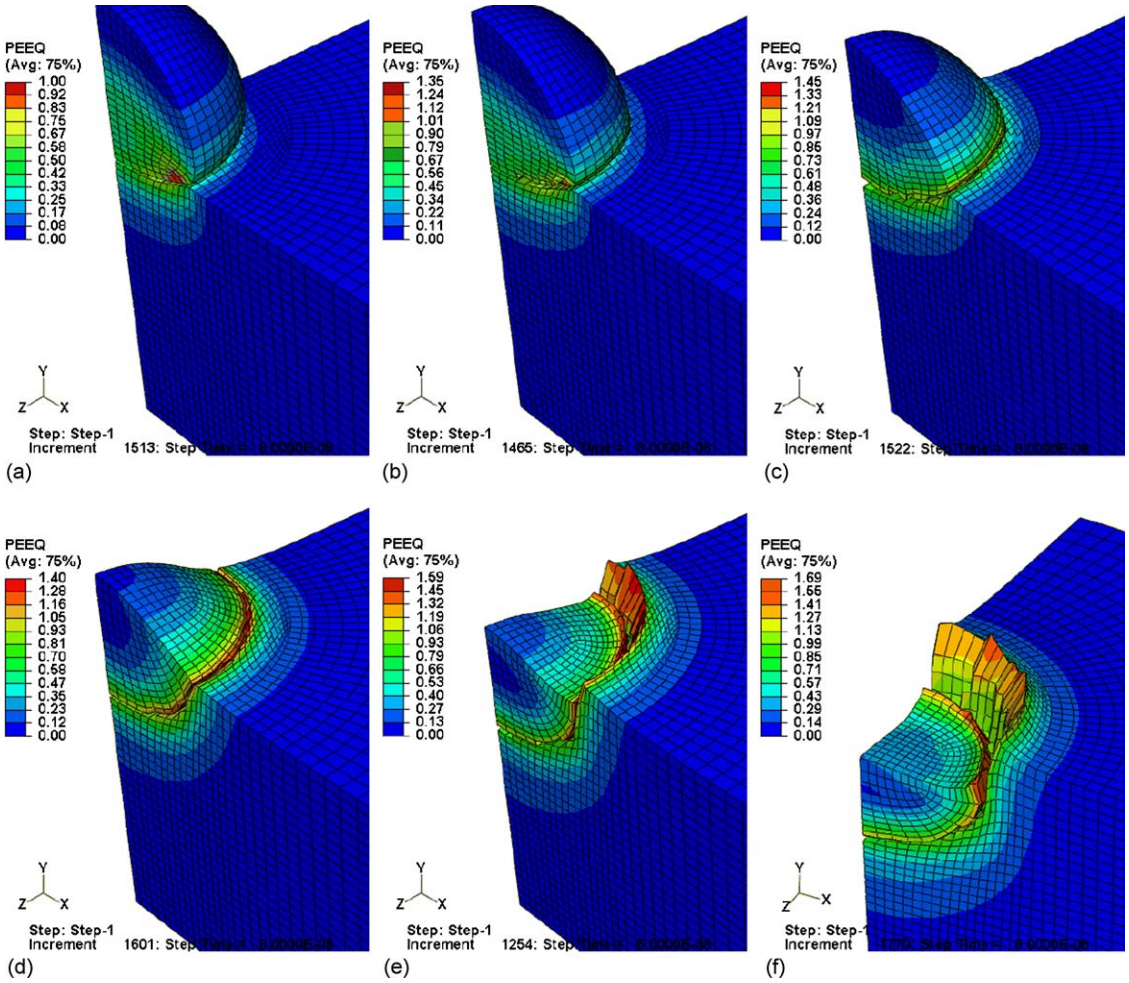

Fig. 12. Simulated contours of PEEQ for a 20 μm Cu particle impacting at 200 m/s (a), 250 m/s (b), 300 m/s (c), 400 m/s (d), 500 m/s (e) and 600 m/s (f). Computed without ALE adaptive meshing, with material damage, a COF of 0.2 and a meshing size of 1 μm ($1/20d_p$).

deformed morphologies, it is found that the depths of craters and the heights of particles are different for three particle sizes, especially when compared 20 μm to 20 mm particles. As the increase of particle size, the depths of craters increase and the heights of particles decrease. This result may be attributed to the influence of a localization of impact kinetic energy on the contact interface, while different particles have different kinetic energies given a velocity. In addition, the kinetic energy is relatively higher than the constant fracture energy no matter the particle sizes. The larger the particle size, the higher the kinetic energy, consequently, the relatively higher concentration of kinetic energy at the contact interface. Therefore, more elements could be deleted in simulations. Moreover, it is worth noting that the deletion of elements occurs as the impact velocity is 200 m/s for 80 μm and 20 mm Cu particles. This fact means that the large particle may need low impact velocity to get deposited. Hence the similarity in the interface region is not suitable. Nevertheless, this may be more close to real case and suggest that the particle size has a little effect on particle deposition. But this effect may be shaded by the effect of surface oxide films in practice. Further experiment is required to support these arguments.

3.3. Discussion on particle deformation and bonding

As has been widely accepted, the deformation behavior of particles takes an important role in a successful particle deposition. The extensive plastic deformation at the contact region can disrupt thin surface oxide films and provide intimate conformal contact of the interfacial fresh metals under high local pressure, thus permitting metallic bonding to occur, as schematically shown in Fig. 15. As the impact progressing, the plastic flow of the interfacial materials extrudes part of the crashed oxide films to the periphery of the contact interface. Therefore, there is still some fine oxide debris residual in the coating [10]. Although the underlying bonding mechanism is still not well understood, the reported bonding strength of cold-sprayed metallic coatings is generally in a range from 10 MPa up to 60 MPa, which may suggest that the mechanical interlocking takes an important role in coating adhesion. Therefore, how much the metallic bonding takes in the cold-sprayed coatings is still unpredictable. Nevertheless, more intensive deformation will normally yield better coating quality. As proposed by Assadi et al. [4] and Grujicic et al. [8], adiabatic shear instability plays an important role in particle/substrate bonding during cold spray deposition. Therefore, it is of significant importance to study the deformation behavior of cold spray particles upon impact.

To characterize the particle deformation extent, flattening ratio (R_f) is used according to the definition in thermal spraying as

$$R_f = \frac{D}{d_p} \tag{5}$$

where D is the spreading diameter of the flattened particle and d_p is the original particle diameter. The spreading diameter means the

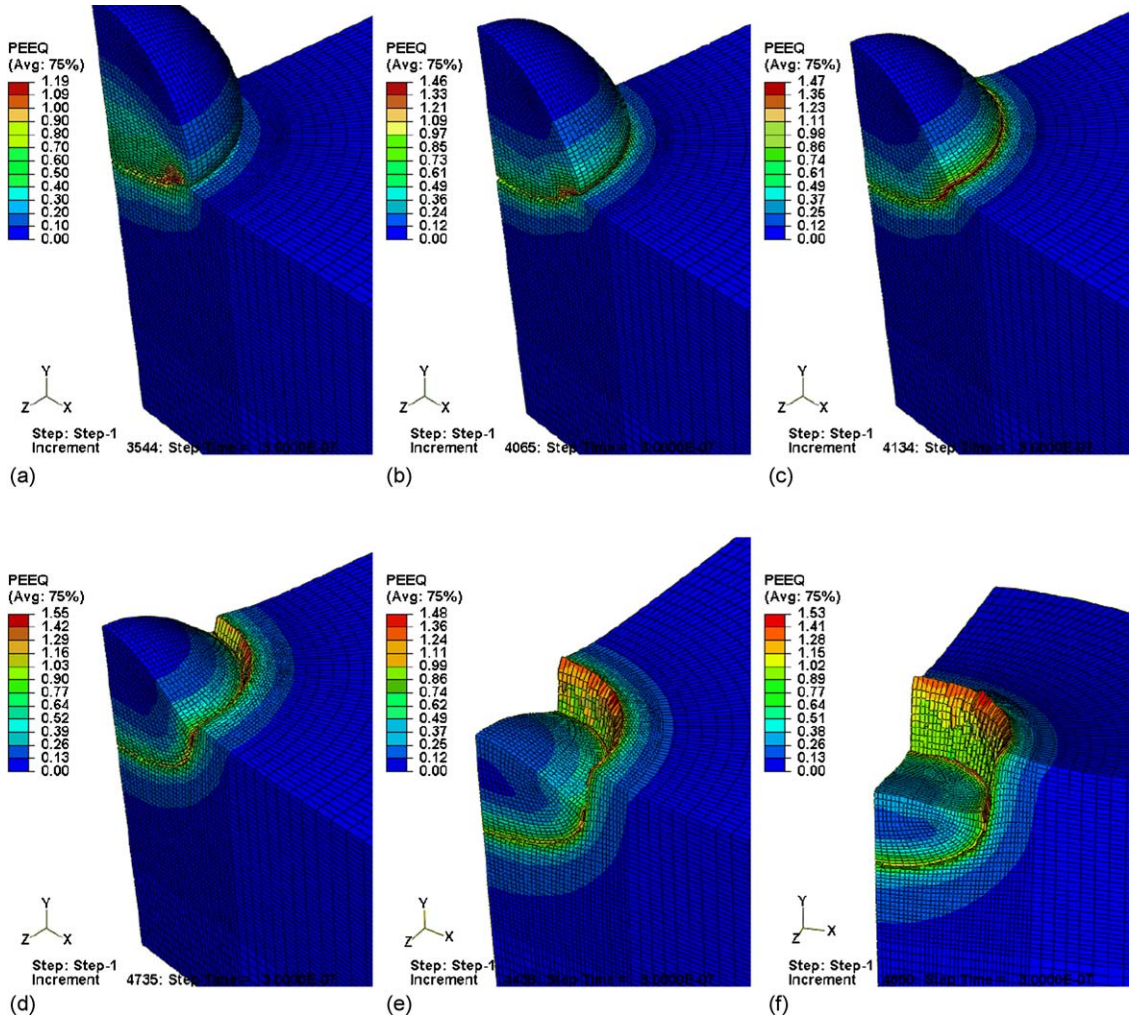

Fig. 13. Simulated contours of PEEQ for a 80 μm Cu particle impacting at 200 m/s (a), 250 m/s (b), 300 m/s (c), 400 m/s (d), 500 m/s (e) and 600 m/s (f). Computed without ALE adaptive meshing, with material damage, a COF of 0.2 and a meshing size of 2 μm ($1/40d_p$).

maximum diameter of the deformed particle perpendicular to impact direction. However, in the previous study it is found that it is difficult to obtain right the spreading diameter in experiments. In addition, in simulations it is also difficult to determine the spreading diameter because of the jet formation. Therefore, the compression ratio (R_c) was developed in the previous study [9], which is defined as

$$R_c = \frac{d_p - h_p}{d_p} \times 100\% \quad (6)$$

where h_p is the height of the flattened particle in the impact direction. It is concluded that the compression ratio is more convenient for characterizing the extent of particle deformation than flattening ratio in numerical study owing to the easy estimation and its independency on meshing size [9].

Fig. 16 shows the predicted compression ratio under different simulation conditions. For comparison, the estimated flattening ratio is illustrated in Fig. 17. The reported experimental values are also given in Figs. 16 and 17. It is seen that the compression ratio increases almost linearly with the increase of particle impact velocity. The compression ratios calculated with material damage are a little higher than those obtained without material damage. In addition, as observed for the particle and crater shapes, the compression ratio increases with increasing the particle diameter because of the deletion of more elements. However, the difference of data obtained under different conditions is relatively small compared to that of the flattening ratios (Fig. 17). On the other hand, the simulated results are comparable to the experimental values taking into consideration the statistical discrepancy.

Through an in-depth analysis, another important issue is presented in Fig. 17 for the flattening ratios. When the impact velocity is low, e.g., less than 250 m/s, the flattening ratios obtained with material damage are similar to those obtained without material damage. When the impact velocity is higher than 250 m/s, the difference between these two kinds of values becomes much larger. This fact is attributed to the deletion of failure elements as the impact velocity is higher than 200–250 m/s depending on the conditions. As mentioned above, the deletion of elements may suggest the shear instability of the interface materials. The shear failure will generate the fresh metals, and thus provide the chance for the particle to be bonded. This may be associated with the critical velocity and will be discussed in the following.

3.4. Discussion on numerical estimation of particle critical velocity

Based on above findings, the onset velocity for the deletion of interface elements may be taken as the so-called critical velocity

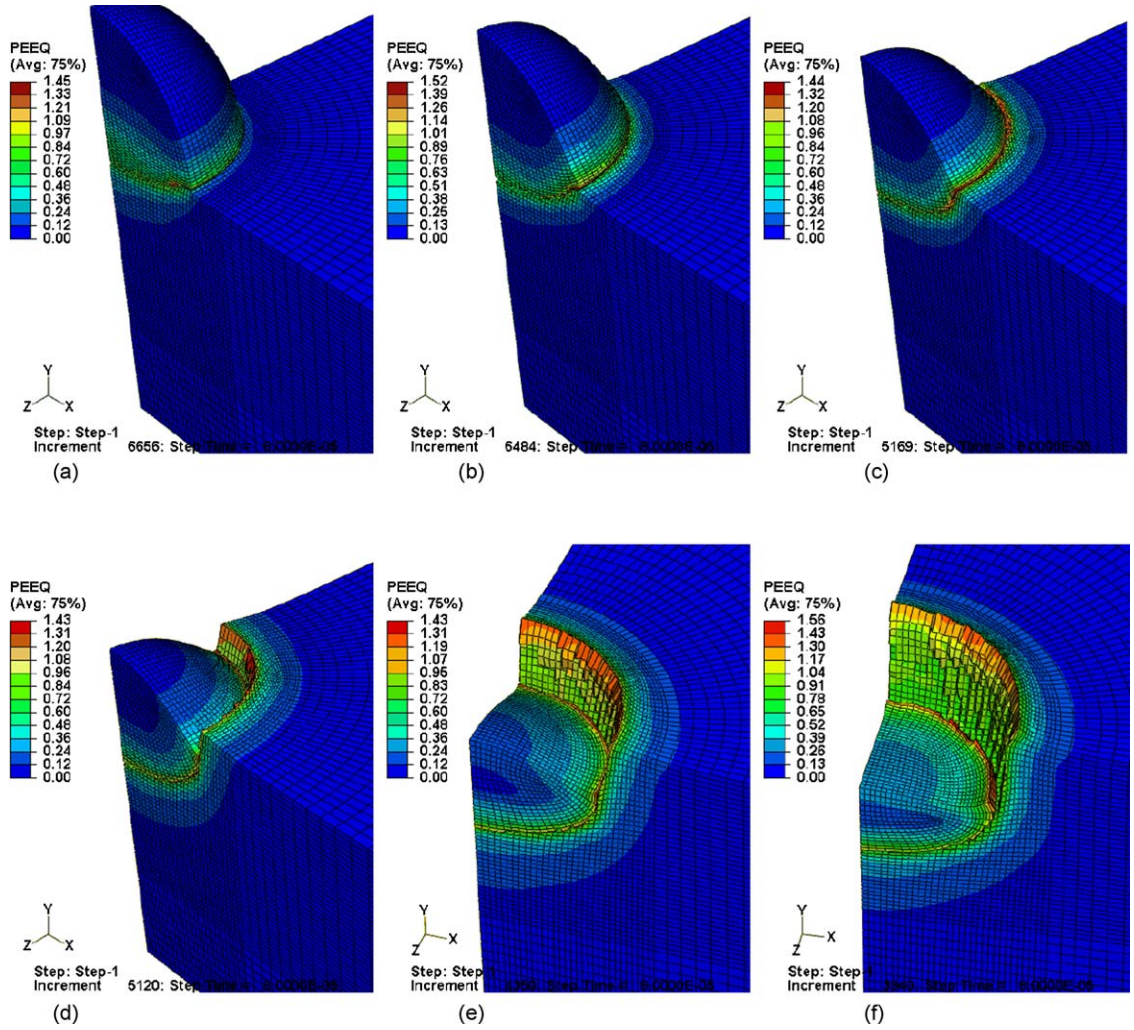

Fig. 14. Simulated contours of PEEQ for a 20 mm Cu particle impacting at 200 m/s (a), 250 m/s (b), 300 m/s (c), 400 m/s (d), 500 m/s (e) and 600 m/s (f). Computed without ALE adaptive meshing, with material damage, a COF of 0.2 and a meshing size of 0.5 mm ($1/40d_p$).

for particle deposition as predicted before [4,6,8,9]. With this in mind and as a first approximation, different impact velocities were calculated with an increment of 10 m/s for different particle sizes. It is also assumed that the critical velocity is estimated when the elements of the first layer in particle surface begin to be deleted. The results are plotted in Fig. 18. For comparison, the reported experimental results [5,6] are also given. It is seen that the critical velocity decreases with increasing the particle size in a large range (20 μm to 20 mm). This means the particle size just has a little effect on the estimated critical velocity. The change trend of the estimated critical velocity for small Cu particles agrees well with the experimental results [5], but the values are much lower than the experimental ones by Schmidt et al. [5]. The estimated critical velocities are from 190 m/s (20 mm) to 230 m/s (20 μm), which is much lower than the reported critical velocities in the literature. According to the previous study [6], a critical velocity of about 300 m/s for Cu powder having low oxygen content was found. Schmidt et al. [5] also reported an adhesion velocity of about 250 m/s for 20 mm Cu spherical projectile. As proposed in the previous study [6], the dominant effect of particle oxidation state

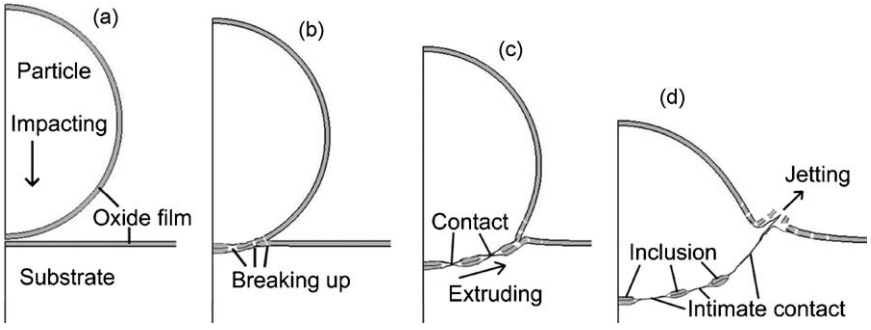

Fig. 15. Schematic diagram of particle impacting and bonding processes in cold spraying.

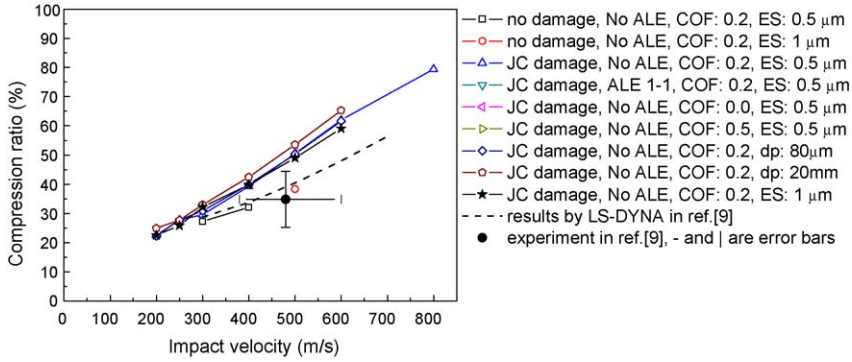

Fig. 16. Change of compression ratio with impact velocity under different conditions.

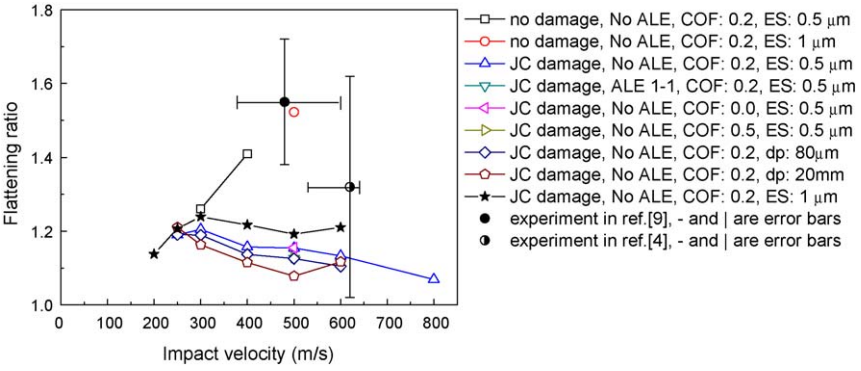

Fig. 17. Change of flattening ratio with impact velocity under different conditions.

could explain well the up-to-date findings by different research groups. Kang et al. [12] later reported the similar oxidation dependency of aluminum powders and proved our model. Therefore, the estimated critical velocity in this study is very reasonable because the effect of oxide films is not considered in simulations.

For validation, 1100-H12 aluminum alloy (commercially pure Al) was adopted and modeled with the developed 3D model. Its properties were taken from Ref. [16]. Fig. 19 shows the typical simulated contours of PEEQ for a 20 μm Al1100 particle impacting upon Al1100 substrate at 300, 350 and 400 m/s. The deformation of Al1100 particle presents a similar tendency with Cu. The deformation extent increases with the increase of impact velocity. The estimation of critical velocity yields a value of about 350 m/s. This value is also much lower than the reported experimentally measured critical velocities of Al powders [5,12]. But Schmidt et al. [5] also reported an adhesion velocity of about 400 m/s for 20 mm Al spherical projectile. Taking into account the special effect of aluminum oxide in Al deposition [10,11], the estimated value is also reasonable.

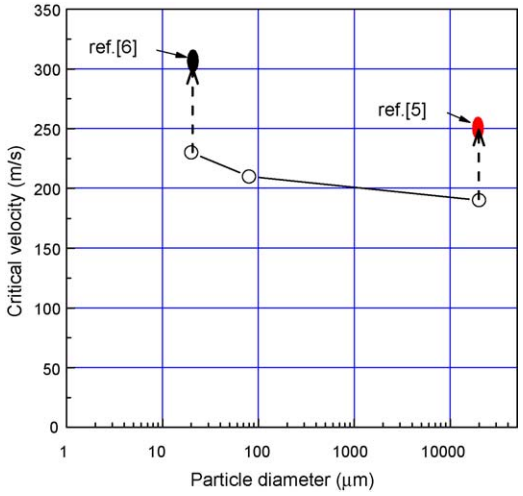

Fig. 18. Change of predicted critical velocity with particle size.

It is worth noting that similar numerical investigations were also performed for other materials, such as Armco iron and 4340 steel whose properties can also be found in Ref. [15]. But the results are not satisfactory because the reported material damage parameters are not suitable for conditions in cold spraying. For example, although 4340 steel has a much higher strength than Cu, a large number of elements are damaged even at a relatively low velocity of 200 m/s due to its lower failure strain [15].

Therefore, the developed 3D simulation procedure with material damage supplies a tool to predict the critical velocity of the metallic materials to be sprayed. However, the material properties used for the current analysis have been based on the data reported for bulk materials [15,16], and for strain rates which are by 6 orders of magnitude smaller than those in cold spraying, in which strain rates can be in the range of 10^8 to 10^9 1/s. To obtain the accurate and/or effective materials properties is very difficult because the deformation conditions in cold spraying are complicated. In addition, the properties of the feedstock powder may deviate substantially from those of bulk materials due to effects, such as grain refinement, from high quenching rates during atomization. Moreover, the oxidation of powder during stocking or in use can also offset the real critical velocity.

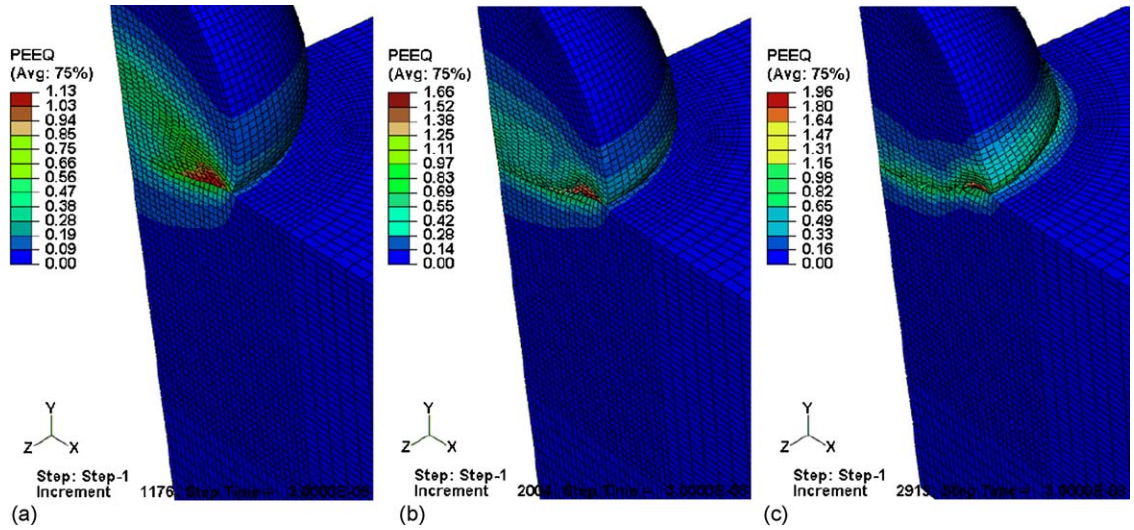

Fig. 19. Simulated contours of PEEQ for a 20 μm Al1100 particle impacting at 300 m/s (a), 350 m/s (b) and 400 m/s (c). Computed without ALE adaptive meshing, with material damage and a COF of 0.2.

4. Concluding remarks

Through the systematic investigation of the effects of the simulation settings on the output in 3D modeling the impacting behavior of cold spray particles, the capability of 3D numerical simulation of particle impacting by the ABAQUS/Explicit program with material damage was evaluated. The results show that the satisfactory output could be obtained with the appropriate settings, but careful regulation of the setting factors is necessary. In addition, the meshing size has less effect on the resultant output with the material damage than without the material damage. Although the particle size has little effect on the deformation behavior of the whole particle, it has some effect on the damage of the contact interface elements. The critical velocity for particle deposition could be estimated given the appropriate material properties. The future work is to investigate more complex impacting conditions (e.g., different temperatures), effect of oxide films, off-normal impact, and multi-particle impact.

Acknowledgements

This work was partially supported by the NPU Talent Development Foundation, the Scientific and Technological Innovation Foundation for Youth NPU Teachers and the Ao-Xiang Star Project.

References

[1] A. Papyrin, Adv. Mater. Process. 159 (2001) 49–51.
[2] T. Stoltenhoff, H. Kreye, H.J. Richter, J. Therm. Spray Technol. 11 (2002) 542–550.
[3] R.C. Dykhuizen, M.F. Smith, D.L. Gilmore, R.A. Neiser, X. Jiang, S. Sampath, J. Therm. Spray Technol. 8 (1999) 559–564.
[4] H. Assadi, F. Gärtner, T. Stoltenhoff, H. Kreye, Acta Mater. 51 (2003) 4379–4394.
[5] T. Schmidt, F. Gärtner, H. Assadi, H. Kreye, Acta Mater. 54 (2006) 729–742.
[6] C.J. Li, W.Y. Li, H.L. Liao, J. Therm. Spray Technol. 15 (2006) 212–222.
[7] M. Grujicic, J.R. Saylor, D.E. Beasley, W.S. DeRosset, D. Helfritch, Appl. Surf. Sci. 219 (2003) 211–227.
[8] M. Grujicic, C.L. Zhao, W.S. DeRosset, D. Helfritch, Mater. Design 25 (2004) 681–688.
[9] W.Y. Li, H.L. Liao, C.J. Li, G. Li, C. Coddet, X.F. Wang, Appl. Surf. Sci. 253 (2006) 2852–2862.
[10] W.Y. Li, H.L. Liao, C.J. Li, H.-S. Bang, C. Coddet, Appl. Surf. Sci. 253 (2007) 5084–5091.
[11] W.Y. Li, C. Zhang, H.T. Wang, X.P. Guo, H.L. Liao, C.-J. Li, C. Coddet, Appl. Surf. Sci. 253 (2007) 3557–3562.
[12] K. Kang, S. Yoon, Y. Ji, C. Lee, Mater. Sci. Eng. A 486 (2008) 300–307.
[13] C.J. Li, W.Y. Li, Surf. Coat. Technol. 162 (2003) 31–41.
[14] Abaqus Analysis User's Manual, ABAQUS 6.7 HTML Documentation, Dassault Systèmes, 2007.
[15] G.R. Johnson, W.H. Cook, Eng. Fract. Mech. 21 (1985) 31–48.
[16] N.K. Gupta, M.A. Iqbal, G.S. Sekhon, Int. J. Impact Eng. 32 (2006) 1921–1944.